

# Investigation of the letrozole interaction with human serum albumin using a combination of MCR-ALS chemometrics, multi-spectrometric and molecular modeling

Parisa GHANDFOROUSHAN<sup>1</sup> , Saheleh SHEYKHIZADEH<sup>2</sup> , Fatemeh POURESHGHI<sup>3</sup> , Mostafa ZAKARIAZADEH<sup>4</sup> , Somaieh SOLTANI<sup>1,\*</sup> 

<sup>1</sup> Department of Drug applied research center, Faculty of Pharmacy, Tabriz University of Medical Sciences University, Tabriz, Iran.

<sup>2</sup> Department of Pharmaceutical analysis research center, Tabriz University of Medical Sciences University, Tabriz, Iran.

<sup>3</sup> Department of materials, Norwegian University of Sciences and Technology (NTNU), NO-7491 Trondheim, Norway

<sup>4</sup> Department of Biochemistry, Faculty of Sciences, Payame Noor University, Tehran, Iran.

\* Corresponding Author. E-mail: soltanis@tbzmed.ac.ir (S.S.); Tel. +98-4113372254.

Received: 26 January 2023 / Revised: 01 April 2023 / Accepted: 01 April 2023

**ABSTRACT:** Letrozole-HSA (human serum albumin) binding was studied using various spectroscopic techniques, MCR-ALS (multivariate curve resolution alternating least squares) chemometrics method, and molecular modelings. Binding constant at different temperatures, main interacted sites properties, thermodynamic parameters, HSA conformation in complex form was obtained using the relevant data. Due to the fluorescence emission wavelength overlap of LET and HSA, fluorescence emission enhancement was seen at the emission wavelength of 340 nm, following the excitation at 278 nm rather than fluorescence quenching. MCR-ALS analysis of UV-Vis absorption and fluorescence emission data approved the complex formation between LET and HSA. The fluorescence emission quenching was observed at 320 nm rather than 340 nm. The emission data were fitted to the Stern-Volmer, van't Hoff, and Hill models to calculate the quenching and binding constants. The results showed that LET binds to HSA with a binding constant of  $2.25 \times 10^4 \text{ M}^{-1}$  that resembles the moderate binding capacity of LET to HSA. Furthermore, decreased binding constant at higher temperatures and decreased quenching constants at higher temperatures showed static quenching constant.

Thermodynamic analysis and simultaneous competitive binding studies showed that LET interacts with HSA's subdomain IIA and IIIA mainly by hydrogen and Van der Waals bonds. The results agree with molecular modeling studies. FTIR and circular dichroism (CD) results revealed the reduced alpha-helical structure of HSA in LET-HSA complex compared to non-bound form.

**KEYWORDS:** Letrozole; Human serum albumin; spectroscopy; MCR-ALS; Emission spectra overlap.

## 1. INTRODUCTION

HSA binds to relatively insoluble substances, including nutrients, hormones, fatty acids, and drugs [1, 2]. Drug pharmacokinetics and pharmacodynamics [3, 4] are significantly influenced by their HSA-binding. There are several albumin-based formulations in the market as well in clinical studies [5, 6]. HSA (585 amino acids), a globular heart-shaped structure protein (Figure 1) that is composed of domains (I (1-195), II (196-383), III (384-585)). Subdomains IIA and IIIA (both with hydrophobic characteristics) are known as drug binding sites I and II, respectively. Environmental factors like pH and ionic strength alter HSA's molecular structure [7, 8].

The molecular interaction mechanism of anticancer drugs with HSA has been studied frequently [9-17]. Bourassa et al. reported the binding of tamoxifen (an anticancer drug is used in breast cancer) and related compounds to HSA in the year 2011 [9] using different spectroscopic methods. Letrozole (LET, Figure 1) is used in breast cancer as an endocrine therapy [18, 19]. The estrogen production is inhibited by LET following

**How to cite this article:** Ghandforoushan P, Sheykhizadeh S, Poureshghi F, Zakariazadeh M, Soltani S, Investigation of the letrozole interaction with human serum albumin using a combination of MCR-ALS chemometrics, multi-spectrometric and molecular modeling. J Res Pharm. 2024; 28(1): 1-15.

inhibition of the aromatase enzyme [20, 21]. The glucuronide metabolite of LET is excreted in the urine [22, 23]. LET binds to HSA approximately 55% [24]. Maliszewska et al. [25] have evaluated the interaction of LET with HSA compared to resveratrol using a fluorometric method, and they concluded that resveratrol binds strongly than LET to HSA.

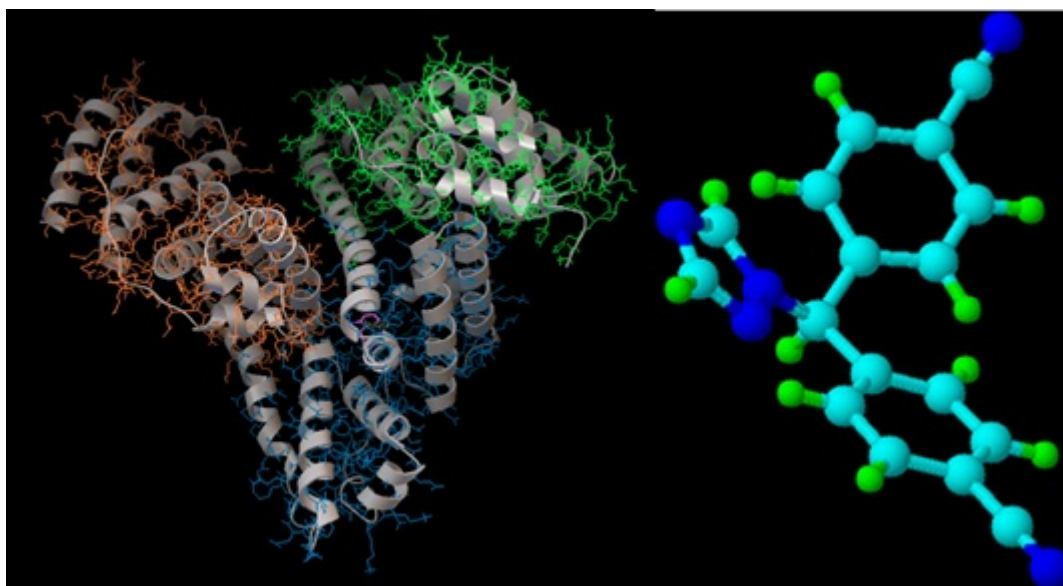


**Figure 1.** Cristal structure of HSA (Trp 214 shown in purple) and 3D molecular structure of LET

In a similar study, Bijari et al. studied the interactions of the LET with HSA utilizing various spectroscopic techniques and docking methods. Despite a notable similarity between our studies, the obtained results do not tell the same story. Interestingly, our results differ from theirs in several aspects, and based on our belief, their findings about the interaction of the LET and HSA have not been correct. The most prominent factor of our study is utilizing MCR-ALS chemometrics and CD analysis. The conflict results of these two studies will be mentioned in the results sections [26].

We investigated the molecular mechanism of LET binding to the HSA using combined multi-spectroscopic techniques, chemometrics models (MCR-ALS), and molecular modeling methods. Spectroscopic methods provide the possibility of interaction dynamics (binding constants and cooperativity) study. The chemometrics method has been used to analyze the fluorescence-visible data of the albumin-drug interaction [27-30]. Our preliminary study shows that the fluorescence emission overlapping between LET and HSA (340-400 nm) leads to the emission enhancement following excitation at 280 nm rather than usual quenching. MCR-ALS chemometrics method was utilized to determine the two-way fluorescence and absorption data of the LET-HSA complex. The quenched emission wavelength region of HSA (320 nm) was used for further binding evaluations. Molecular modeling studies were utilized to evaluate the mode of LET-HSA interaction [8, 31-36].

## 2. RESULTS AND DISCUSSION

### 2.1. UV absorption spectra

UV-Vis spectra of HSA and HSA-LET ( $4 \times 10^{-6}$  M to  $3.5 \times 10^{-5}$  M) are shown in Figure 2. The HSA'S maximum wavelength peak (280 nm) increased due to the complex formation with LET. A minor shift of the LET-HSA spectrum toward longer wavelengths (red-shift) was observed, which could be due to the complex composition amid LET and HSA. Increased hydrophobicity of the binding site microenvironment following the complex formation (because of minor conformational changes in HSA) could be a reason for this wavelength shift.

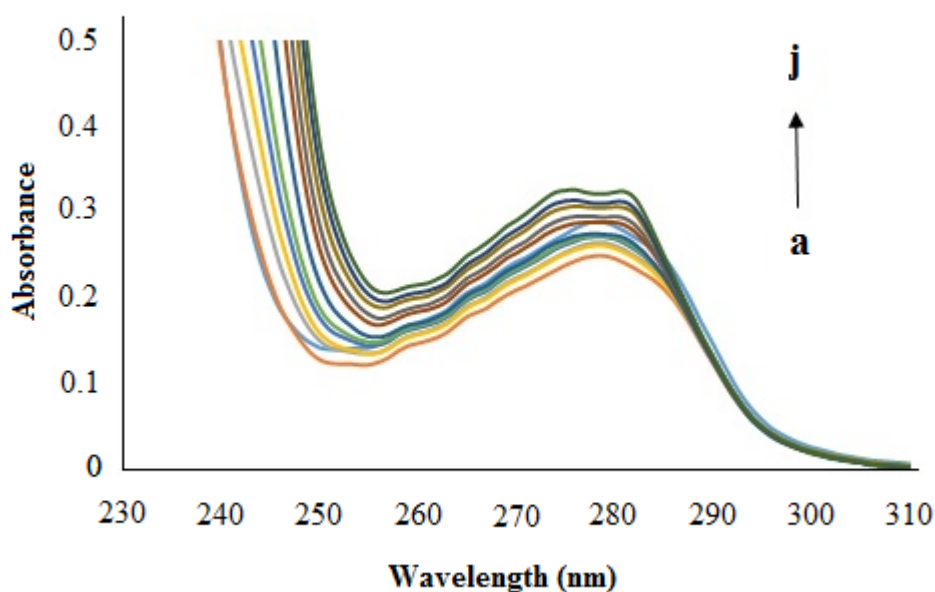


**Figure 2.** The UV absorption spectra of LET-HSA in aqueous solution under the optimum conditions (pH 7.4, ionic strength 0.15 M) at  $T = 298$  K. The  $[HSA]$  was  $6.66 \times 10^{-6}$  M, and the  $[LET]$  was  $4 \times 10^{-6}$  M to  $3.5 \times 10^{-5}$  M from *a* to *j* (there are 8 samples).  $[LET] = 0, 4 \times 10^{-6}, 8 \times 10^{-6}, 1.0 \times 10^{-5}, 1.5 \times 10^{-5}, 2.0 \times 10^{-5}, 2.5 \times 10^{-5}, 3.0 \times 10^{-5}, 3.5 \times 10^{-5}$  M.

## 2.2. Binding mechanism and binding constants

### 2.2.1. Fluorescence spectra

HSA holds 17 tyrosyl residues and one tryptophan (Trp214) residue (Figure 1), while the HSA's emission at 340 nm ( $\lambda_{ex} = 280$  nm) originates mainly from Trp214. The fluorescence intensity of HSA ( $6.66 \times 10^{-6}$  M) and HSA-LET complexes have been displayed in Figure 3. The shift of maximum emission wavelength (347 to 355) occurred due to the complex formation with LET, resulting from polarity enhancement of the fluorophore microenvironment. The LET emission spectra overlap with HSA's emission (340-350 nm), as shown in Figure 3. Consequently, the increasing emission intensity of the HSA (340 to 355 nm) cannot be attributed to the amplification of HSA's emission following the LET-HSA binding.

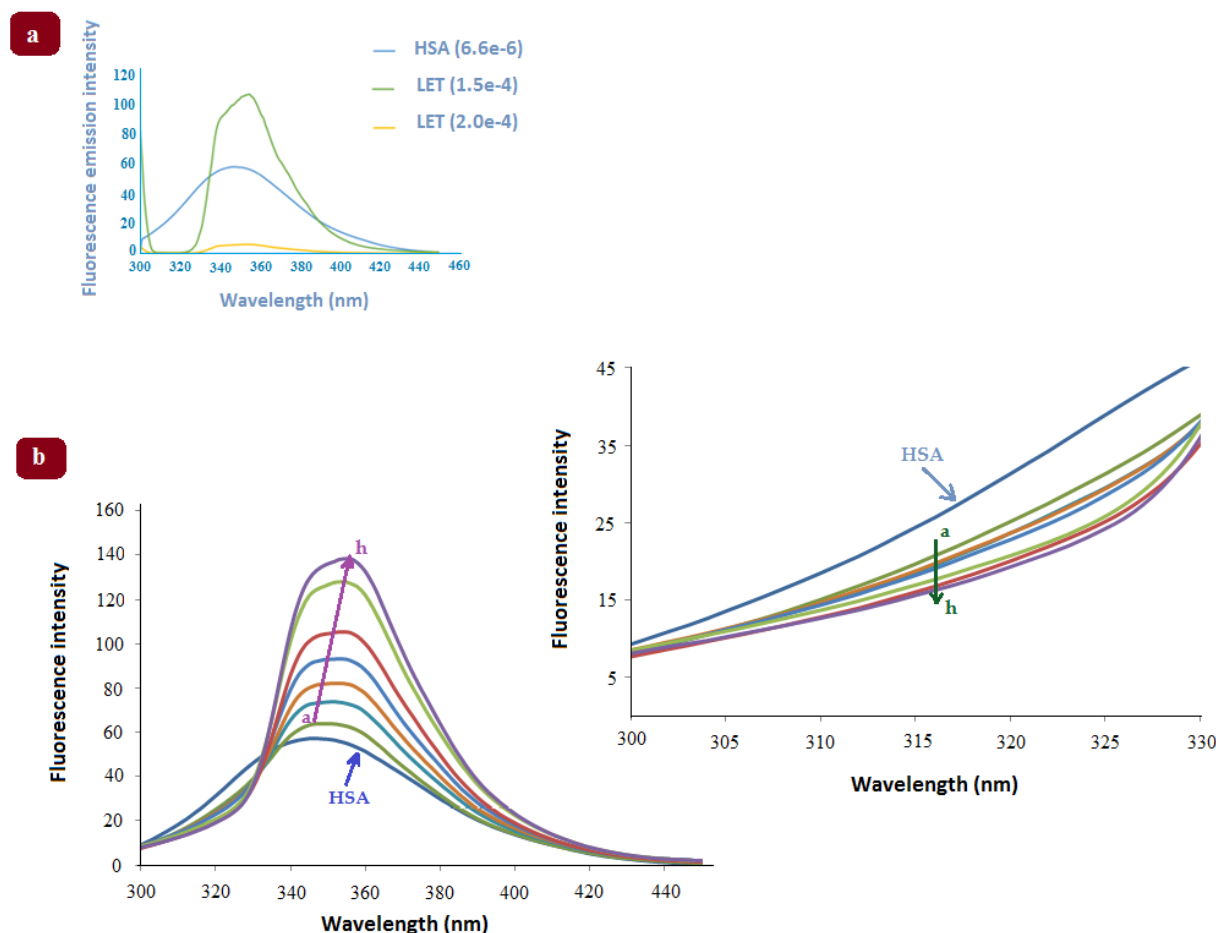


**Figure 3.** a) Fluorescence emission spectra of HSA and letrozole;  $\lambda_{ex}=280$  nm, pH=7.4, Buffer= 0.1M, T=298K,  $C_{Letrozole} = 1.5 \times 10^{-4}$  M,  $C_{Letrozole} = 2.0 \times 10^{-4}$  M,  $C_{HSA} = 6.66 \times 10^{-6}$  M. The LET emission spectra overlap with HSA's emission in the range of 340-350 nm. b) The fluorescence emission spectra of HSA-LET in phosphate buffer (pH 7.40) at T = 298° K. The [HSA] was  $6.66 \times 10^{-6}$  M, and the [LET] was 0 -  $3.5 \times 10^{-4}$  M from a to h. [LET]= 0,  $4 \times 10^{-6}$ ,  $8 \times 10^{-6}$ ,  $1.0 \times 10^{-5}$ ,  $1.5 \times 10^{-5}$ ,  $2.0 \times 10^{-5}$ ,  $2.5 \times 10^{-5}$ ,  $3.0 \times 10^{-5}$ ,  $3.5 \times 10^{-5}$  M. (The third graph is an enlarged part corresponding to the initial part of the graph, which shows the decreasing trend of fluorescence intensity [LET] in the range of 300-330 nm).

The fluorescence emission elevation in the range of 335-410, and HSA fluorescent emission quenching due to the complex formation with LET from 310-335 nm. This overlap region was analyzed by MCR-ALS, which is described in the 4.2.2 section. Also, to avoid the fault results, the calculation of quenching parameters was investigated in a non-overlapped region ( $\lambda_{em} = 320$  nm).

### 2.2.2. MCR-ALS optimization

$D_{aug}$  was obtained from combined UV-Vis and fluorescence measurements (Eq. 9). Singular value decomposition (SVD) was applied to ascertain the species. The HSA's and LET's spectra were utilized as the initial estimates for the MCR-ALS optimization model. Unimodality of concentration profiles and non-negativity in the studied profiles were utilized as constraints. As perceived from the SVD analysis,  $D_{aug}$  data, three singular values covered more than 99% of the variance. It is rational to state that three singular values were regarded as free LET, free HSA, and HSA-LET complex species. Figure 4 shows obtained concentration and spectra profiles for  $D_{aug}$  that were tough to achieve by conventional procedures.

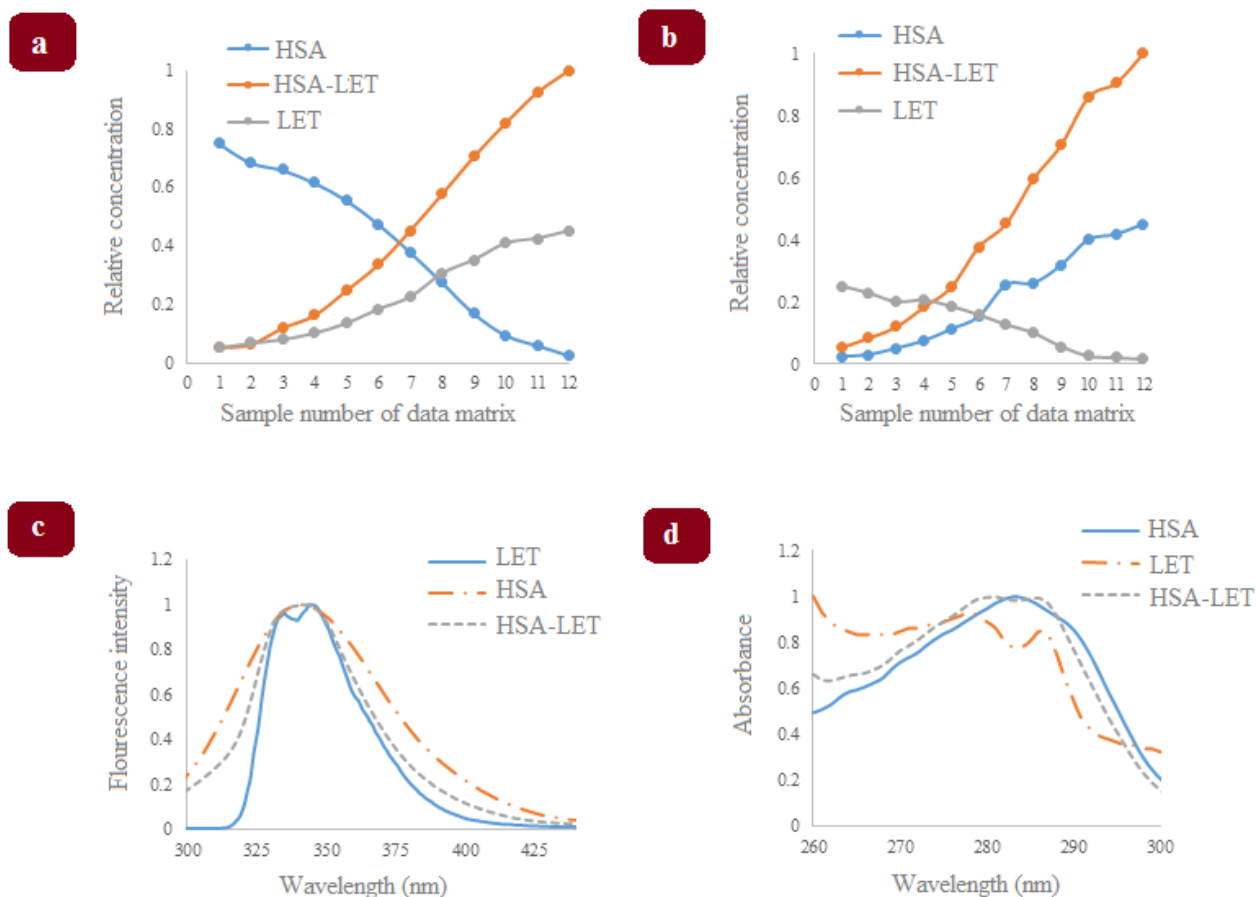


**Figure 4.** The resolved concentration and spectral profiles of equilibrium species were obtained by applying MCR-ALS to augmented data matrix: (a) and (b) concentration profiles of species involved. (c), and (d) spectral profiles of species involved in fluorescence and UV-Vis experiment, respectively.

As shown in Figure 4a, by increasing LET concentration, HSA profiles concentration reduced, which is related to the HSA-LET complex formation, and increasing LET concentration profiles is attributable to the free LET. In the other mod, it can be observed that increasing in HSA concentration caused reducing in LET's concentration profiles due to the HSA-LET formation. Increased HSA's concentration profiles attribute to the HSA (Figure 4b). Figures 4c and 4d represent the resolved emission and absorption profiles of LET, HSA, and HSA-LET. The resolved spectra qualitatively explain the studied species' spectral characteristics; according to obtained LOF ( $0.39\% < 5\%$ ), it can be said that almost all variability of the data has been modeled.

### 2.2.3. Elimination of the inner filter effects

Equation (1) was employed to correct the fluorescence intensities by reducing the inner filter effect [37].

$$F_{\text{cor}} = F_{\text{obs}} \times e^{(A_{\text{ex}} + A_{\text{em}})/2} \quad (\text{Eq. 1})$$

Where  $F_{\text{obs}}$  and  $F_{\text{cor}}$  represent the detected and the corrected fluorescence intensity. UV absorbance intensity at emission wavelength and excitation wavelength of LET has been shown by  $A_{\text{em}}$  and  $A_{\text{ex}}$ , respectively.

### 2.2.4. Quenching mechanism study

The corrected fluorescence emission data were fitted to the Stern-Volmer equation (Eq.2) [34].:

$$F_0 / F = 1 + K_{\text{SV}}[Q] = 1 + k_q \tau_0 [Q] \quad (\text{Eq. 2})$$

Where  $F$  and  $F_0$  are the emission intensity of LET-HSA and only HSA while LET plays the quencher  $[Q]$  role, respectively.  $K_{SV}$  ( $M^{-1}$ ) and  $k_q$  ( $M^{-1}s^{-1}$ ) describing the quenching constant and the quenching rate constant, respectively.  $\tau_0$  is the fluorescence lifetime of HSA ( $10^{-8} s^{-1}$ ). The  $K_{SV}$  is the slope of the  $F_0/F$  plot versus  $[Q]$ . The obtained curves at elevated temperatures are shown in Figure 5a.

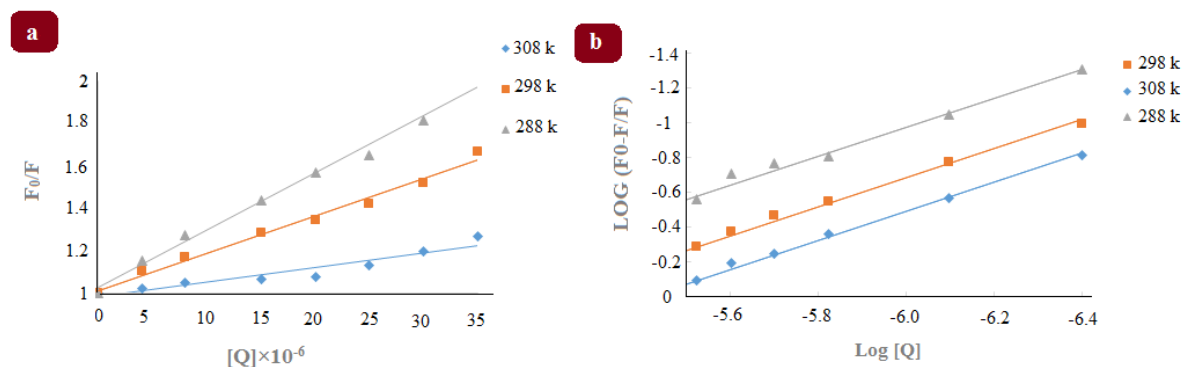


**Figure 5.** (a) Stern – Volmer plots for HSA-LET system at different temperatures, (b) plots of  $\log(F_0-F/F)$  vs.  $\log [Q]$  for the quenching of HSA by LET at different temperatures.  $[LET] = 0, 4 \times 10^{-6}, 8 \times 10^{-6}, 1.0 \times 10^{-5}, 1.5 \times 10^{-5}, 2.0 \times 10^{-5}, 2.5 \times 10^{-5}, 3.0 \times 10^{-5}, 3.5 \times 10^{-5} M$ .

The linear behavior of the  $F_0 / F$  plot versus  $[Q]$  shows that the quenching mechanism is static. The obtained  $K_{SV}$  ( $1.72 \times 10^5 M^{-1}$ ) at 298 K describes the high quenching capability of LET. The calculated  $k_q$  at 298 K was  $1.72 \times 10^{13} M^{-1} s^{-1}$  (Table 1), higher than the maximum diffusion collision quenching rate constant ( $2 \times 10^{10} M^{-1} s^{-1}$ ), which describes a static quenching mechanism.

**Table 1.** The quenching and relevant thermodynamic parameters for the HSA–LET system at different temperatures.

T (K)	$K_{SV} \times 10^5 (M^{-1})$	$K_b \times 10^4 (M^{-1})$	n	$\Delta H$ (kj mol <sup>-1</sup> )	$\Delta S$ (j mol <sup>-1</sup> K <sup>-1</sup> )	$\Delta G$ (kj mol <sup>-1</sup> )
288°	2.72	3.46	0.94			-37.59
298°	1.73	2.25	0.88	-38.95	-47.79	-37.54
308°	0.67	1.23	0.84			-37.50

The binding constant ( $K_b$ ) and cooperativity ( $n$ ) calculated utilizing the Hill method (Eq.3) [33]:

$$\log \frac{(F_0 - F)}{F} = \log K_b + n \log [Q] \quad (\text{Eq.3})$$

$K_b$  at 298 K was  $2.25 \times 10^4 M^{-1}$  that resembles the moderate HSA binding capability of LET. The results showed that  $K_b$  decreased at higher temperatures (Figure 5b, Table 1). The number of binding sites ( $n$ ) was lower than 1 at all studied temperatures (Table 1), representing the negative cooperation of LET molecules while interacting with HSA. The reduced  $n$  values and increased negative cooperation at higher temperatures are shown in Table 1. These findings could be a result of decreased stability of the LET-HSA complex at higher temperatures.

### 2.2.5. Thermodynamic data analysis

Electrostatic, van der Waals, hydrophobic interactions, and hydrogen bonds contribute as main binding forces in drug-protein complex formation [38]. The nature of the dominant forces could be investigated using thermodynamic characteristics of LET-HSA's complex. The obtained binding constants were fitted to the Van't

Hoff model (Equation 4) and the change in enthalpy ( $\Delta H$ ) and entropy ( $\Delta S$ ) were computed from the slope and intercept.

$$\ln K = -\frac{\Delta H}{RT} + \frac{\Delta S}{R} \quad (\text{Eq. 4})$$

The calculated  $\Delta H$  and  $\Delta S$  were  $-38.95 \text{ kJ mol}^{-1}$  and  $-47.79 \text{ J mol}^{-1} \text{ K}^{-1}$ , implying the contribution of the hydrogen bonding and van der Waals forces as the leading players of LET-HSA complex formation [39].

$\Delta G$  was obtained using the Gibbs model (equation 5):

$$\Delta G = \Delta H - T\Delta S \quad (\text{Eq.5})$$

The negative value for  $\Delta G$  of LET binding to HSA (Table 1) approves that the binding happened spontaneously. The resulted  $\Delta G$  values were not significantly changed in the studied temperature range, while a slow reduction was observed at higher temperatures.

In comparison with Bijari et al. investigation, although the thermodynamic parameters' profiles are similar to each other (E.g., negative  $\Delta H$ ,  $\Delta S$ , and  $\Delta G$ ), there is a remarkable contrast between the obtained quantities. Moreover, the quantities of the KSV and  $K_b$  show notable differences (E.g.  $3.46 \times 10^4$  vs.  $31.62 \times 10^{-4} \text{ M}^{-1}$  for  $k_b$  and  $2.72 \times 10^4$  vs.  $67.47 \times 10^{-4} \text{ M}^{-1}$  for KSV) [26].

### 2.3. Site marker competitive binding experiments

Drugs competitively bind to the known drug binding sites of HSA. Warfarin and Ibuprofen (specific markers of site I and site II) were utilized for LET binding site evaluations. Figure 6 shows the Stern-Volmer diagrams of LET-HSA, LET-Warfarin-HSA, LET-Ibuprofen-HSA. Both Warfarin and Ibuprofen lead to a meaningful reduction in binding constant, while the reduction was slightly more substantial for Ibuprofen. The results showed that LET could bind to both sites.

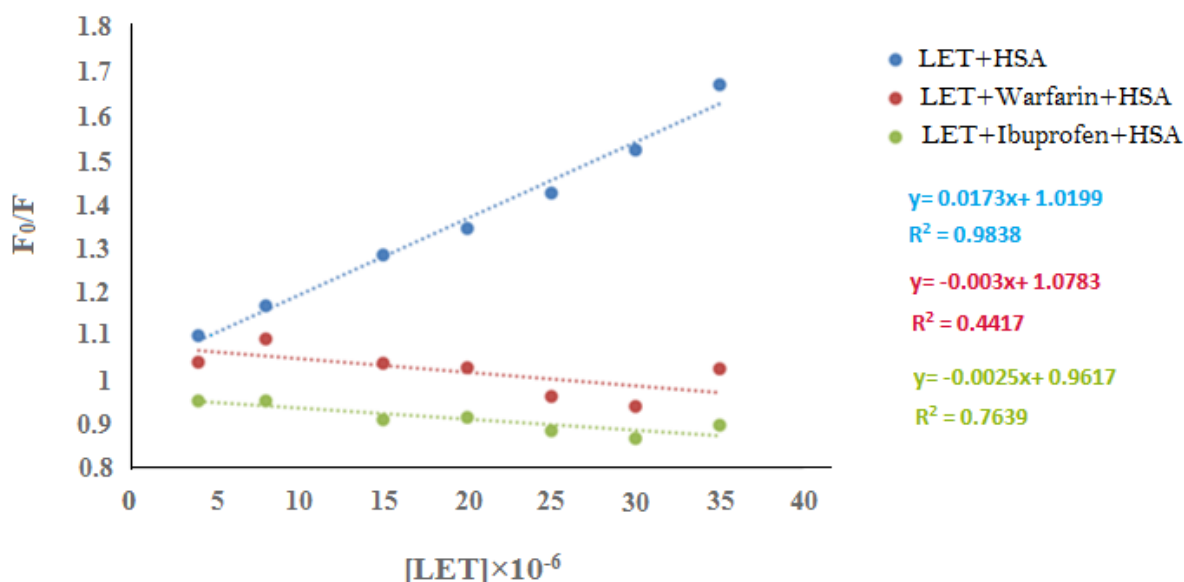


**Figure 6.** Stern-Volmer plots of LET interaction with HSA in the presence and absence of binding site markers (Warfarin and Ibuprofen). [LET] = 0,  $4 \times 10^{-6}$ ,  $8 \times 10^{-6}$ ,  $1.0 \times 10^{-5}$ ,  $1.5 \times 10^{-5}$ ,  $2.0 \times 10^{-5}$ ,  $2.5 \times 10^{-5}$ ,  $3.0 \times 10^{-5}$ ,  $3.5 \times 10^{-5} \text{ M}$ .

## 2.4. Conformational study using ATR-FTIR and CD spectroscopy

### 2.4.1. ATR-FTIR spectra analysis

ATR-FTIR spectra present amide bands of HSA in wavelength numbers ranging from 1600 to 1700  $\text{cm}^{-1}$  [40]. The absorption of protein amide bands can be affected by alteration of their secondary structure and by the presence of water molecules ( $\text{H}_2\text{O}$ ). Although the presence of water could interfere with ATR-FTIR results, it can provide a more native environment [41, 42].

Figure 7 shows the FTIR-ATR spectrum of the HSA and HSA-LET complex. The peak attributed to the amide I have moved from 1656.91 to 1653.74  $\text{cm}^{-1}$ . Furthermore, the position of amide II was moved from 1599.25 (HSA) to 1543.07  $\text{cm}^{-1}$  (HSA-LET). Altered peak positions, shape, and intensity, especially in bands between 1600.0  $\text{cm}^{-1}$  and 1700.0  $\text{cm}^{-1}$ , demonstrate that LET induces alteration of HSA's  $\alpha$ -helical structure.

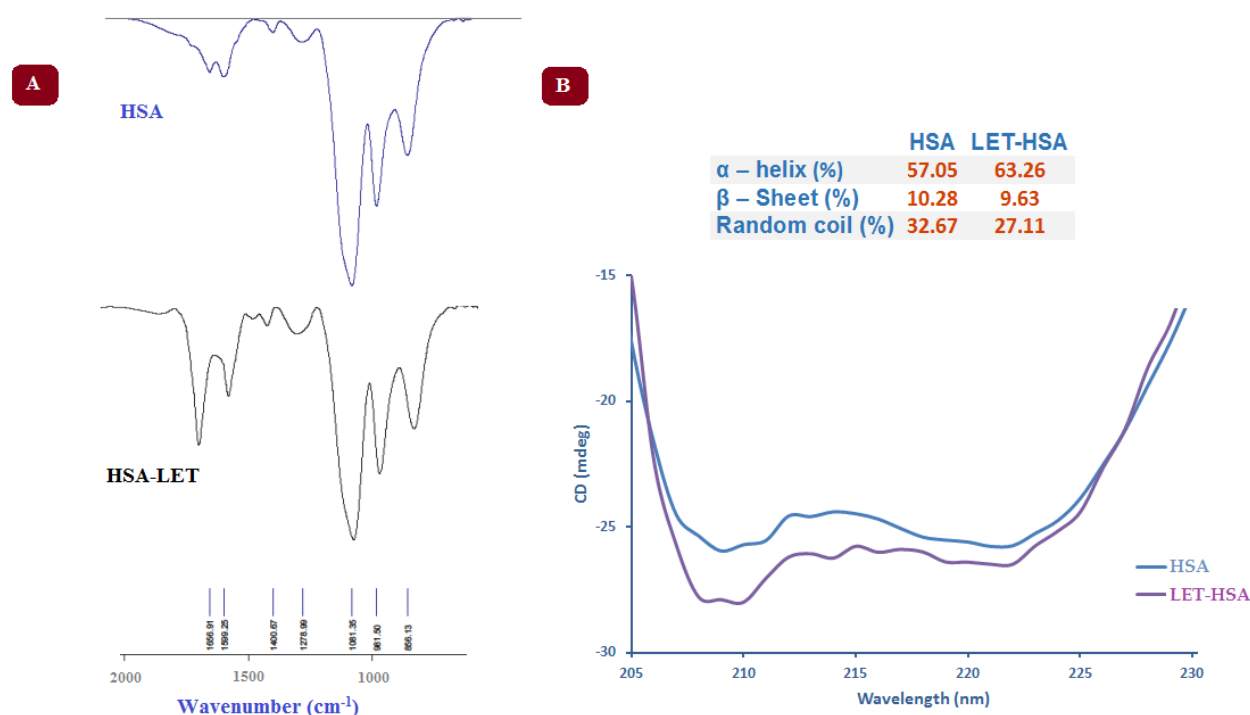


**Figure 7.** (A) FTIR-ATR spectra of HSA and LET-HSA (1:1) in the wavenumber range (2000-663  $\text{cm}^{-1}$ ). (B) CD spectra (200-260 nm) of HSA and the LET-HSA complex.  $C_{\text{HSA}} = 0.025 \text{ mM}$ , pH 7.4,  $T = 298 \text{ K}$ .

### 2.4.2. CD spectra analysis

The CD spectrum of HSA (Figure 7B) (200–260 nm) showed two negative double-humped peaks at 208 and 222 nm, which were attributed to  $n \rightarrow \pi^*$  transfer for the  $\alpha$ -helix structure [33].

Mean residue ellipticity (MRE) for the CD spectra were estimated using equation 6:  $\text{MRE} (\text{deg cm}^2 \text{dmol}^{-1}) = \frac{\text{Observed CD (m deg)}}{C_{\text{pnl}} \times 10}$  (Eq. 6)

In this equation,  $C_p$  is the protein molar concentration,  $n$  is the number of amino-acid residues (585).  $l$  represents the length of the cell (0.1 cm).

The LET binding to HSA (Figure 7B) reduced the MRE of HSA without a significant shift in the band shape. Increasing in the  $\alpha$ -helix% from 57.05% (HAS) to 63.26% (LET-HAS) and a slight decreasing of  $\beta$ -sheets were observed. Similar results with FTIR confirmed the conformational secondary structure changes of HSA due to LET binding.

## 2.5. Molecular modeling

The molecular modeling results are displayed in Figure 8. The docking results (the lowest binding energy value and interacted residues) are shown in Table 2.

**Table 2.** The HSA residues implicated in LET-HSA interaction with the binding energy values for the fittest selected docking sites at two LET sites.

Complex	Residues involved in the interaction	Binding Energy (Kcal mol <sup>-1</sup> )
LET-HSA (Site I)	Lys-195, Gln-196, Cys-245, Tyr-150, Cys-253, His-242	- 8.2
LET-HSA (Site II)	Met-446, Arg-485, Pro-384, Leu-453, Ala-449, Leu-387, Ser-342, Ile-388	-9.6

The models showed that LET has two binding sites surrounded by related amino acid residues, summarized in Table 2. Figure 8 shows the interaction of LET with HSA. LET is located within the hydrogen binding distance of His-242 at site I and Ser-342 at site II (pointed by the red circle in Figure 8). The importance of hydrogen bonds in the binding mechanism is obtained from the results of this study. The nitrogen atoms of nitrile groups and triazole moiety formed hydrogen bonds (green dashed line). Besides it, aromatic benzene rings of LET facilitate the hydrophobic interactions (red spoked arcs) (Figure 8). According to the results, LET binds to both sites I and II. On the other hand, Bijari et al. reported only one site interaction (Site I) for LET. According to Table 2 our results represents lower binding energy (-8.2 (Site I), -9.6 (Site II) Kcal mol<sup>-1</sup>) compared to Bijari et al. publication (-6.94 Kcal mol<sup>-1</sup>) [26].

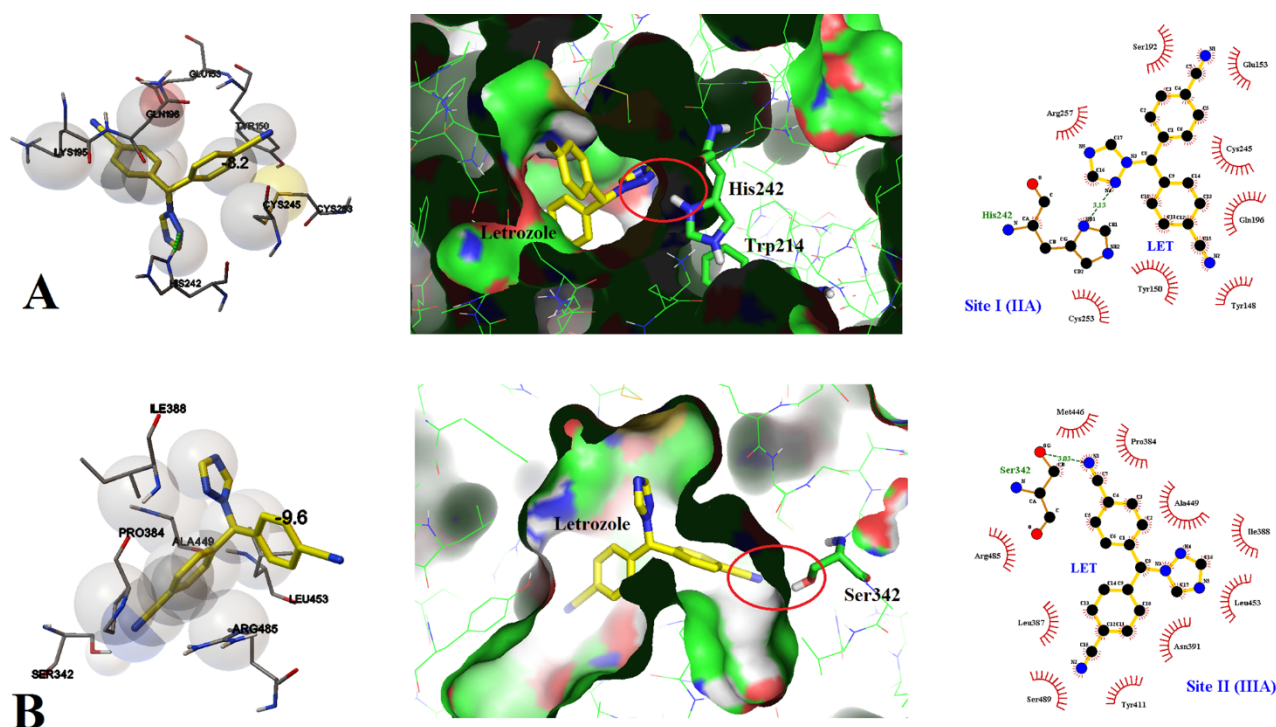


**Figure 8.** 2D and 3D representations of docked poses of LET and HSA. Sites I and II are shown in A, B. The dashed line shows the hydrogen bond.

### 3. CONCLUSION

The binding mechanism of LET to HSA in physiological conditions has been investigated by MCR-ALS combined with spectroscopic and molecular modeling methods. Fluorescence and absorption enhancement analysis has confirmed the formation of the HSA-LET complex, which was subsequently approved by Fluorescence thermodynamics analysis. Nowadays, the utilization of chemometrics methods to extract information from intricate computations has been relatively widespread. The MCR-ALS was utilized to resolve the spectral overlapping of the LET-HSA system. The augmented data matrix of fluorescence spectra and UV-Vis spectra were analyzed with MCR-ALS and extracted from the overlapped region's pure spectra and concentration profiles. Negative enthalpy and entropy change revealed van der Waals forces and hydrogen bonding as dominant binding forces. Negative  $\Delta G$  showed that the complex formation is spontaneous. The results showed that LET moderately binds to the HSA while causing the reduced polarity in the micro-environment of the Trp214 residue. CD and FTIR revealed a LET-induced alteration in HSA's conformation, along with the increase of  $\alpha$ -helix and loss of  $\beta$ -sheet content. The results based on site marker competition revealed that LET binds to site I (subdomain IIA) and site II (subdomain IIIA) of HSA while binding to site II is more potent than other sites. Molecular modeling results showed that LET binds to site I and II through hydrogen bonds and hydrophobic interactions.

### 4. MATERIALS AND METHODS

#### 4.1. Materials

HSA (>97%, 66,000 Da) was acquired from Sigma Chemical Company and then employed as obtained. LET was kindly gifted by Soha pharmaceutical company, Iran, in pure form. Daily prepared deionized water and analytical grade reagents were employed for whole experiments. The water utilized for this project is doubled distillation and prepared daily.

##### 4.1.1. Stock solutions

HSA ( $10^{-4}$  M) was solubilized in phosphate buffer (10 mM, pH 7.4). LET, Ibuprofen, and Warfarin ( $3.0 \times 10^{-3}$  M) in DMSO were stored in the refrigerator ( $0-4^{\circ}\text{C}$ ) until use. Phosphate buffer (pH 7.4, 0.15 M) was utilized to prepare daily solutions.

#### 4.2. Data measurement

##### 4.2.1. Absorption spectroscopy

The UV-Vis spectra were read by a double beam Shimadzu 1800 (Shimadzu, Tokyo, Japan), in the range of 200–400 nm, at  $298^{\circ}\text{K}$ . The UV-Vis spectra were obtained after the addition of elevated drug concentrations. The HSA concentration was set at  $6.66 \times 10^{-6}$  M, while LET was changed from 0 to  $3.5 \times 10^{-4}$  M.

##### 4.2.2. Fluorescence spectroscopy

The emission spectra of HSA ( $6.66 \times 10^{-6}$  M) with increasing LET concentrations (0 to  $3.5 \times 10^{-5}$  M) were obtained (300–450 nm, Jasco spectrofluorometer). The excitation wavelength was 280 nm, and the slit widths were 10/10 nm. Also, HSA-LET interaction was evaluated at elevated temperatures ( $288^{\circ}$ ,  $298^{\circ}$ , and  $308^{\circ}\text{K}$ ), and the data fitted to the van't Hoff model to calculate the thermodynamic constants. The temperature was monitored using a Neslab RTE-110 circulator.

##### 4.2.3. FTIR spectroscopic measurements

FTIR-ATR (Nicolet-6700) spectra of HSA-LET and HSA were obtained under the resolution of  $4\text{ cm}^{-1}$  ( $400-4000\text{ cm}^{-1}$ ) at  $298^{\circ}\text{K}$ . The contributions to buffer and free LET absorbance was digitally subtracted from the results.

#### 4.2.4. Circular dichroism (CD)

A Circular Dichroism Spectrometer (Aviv, USA) was employed to record the CD Spectra studied solutions. Far-UV region (190-260 nm) determinations were done utilizing a quartz cell (0.01 cm). All experiments were done in a nitrogen atmosphere. LET (i.e. 0.125, 0.25 and 0.5 mM) were added to HSA solution (12.5  $\mu$ M). Using the Jasco standard analysis software, conversion of signals to the Mol CD ( $\Delta\epsilon$ ) was carried out. K2D3 online webserver was used to calculate the  $\alpha$ -helix and  $\beta$ -strands [43].

#### 4.2.5. Site marker competitive experiments

The LET binding site on HSA was assessed based on its competition with Warfarin and Ibuprofen in HSA binding. Equimolar concentrations of LET were mixed with HSA/site markers ( $6.66 \times 10^{-6}$  M) solution. After a 15-minute incubation at room temperature, emission spectra were obtained.

#### 4.2.6 Data matrix for MCR-ALS

The following experiments were performed to prepare the needed datasets. To prepare the first dataset, LET elevated concentrations (0 to  $3.5 \times 10^{-5}$  M) were added to the HSA solution ( $6.66 \times 10^{-6}$  M). The second data set was obtained by adding the HSA enhanced concentration ( $0.2 \times 10^{-5}$  M) to the LET solution ( $2 \times 10^{-5}$  M). The UV-Vis spectra (260-300 nm) and fluorescence emission spectra (300 - 450 nm) were recorded. Four data matrices  $D_{UV}^{HSA}$  (12 $\times$ 41),  $D_{UV}^{LET}$  (12 $\times$ 41)  $D_F^{HSA}$ (12 $\times$ 151) and  $D_F^{LET}$  (12 $\times$ 151), were obtained from these measurements.

### 4.3. Molecular modeling

The AutoDock Vina software [44] was used for molecular docking of LET binding with HSA (PDB ID code: 1N5U) [45]. LET 3D geometry structure was drawn and optimized using Hyperchem 8 software [35, 46]. Before docking, the crystallographic structures such as cofactor (heme), ligands, and water molecules were extracted, and the HSA's structure modification was performed by adding the Kollman charges and polar hydrogens. The molecular docking area was fixed by setting up a grid box with a grid box size  $27.75 \times 27.75 \times 27.75 \text{ \AA}^3$  and  $28.50 \times 28.50 \times 28.50 \text{ \AA}^3$  for the binding site I and II, respectively. The grid spacing size is 1.0  $\text{ \AA}$  at Vina docking. The confirmation of LET-HSA complexes with the lowest binding energy conformer was further analyzed with Auto Dock Tools 1.5.6 and LigPlot+ v 1.4.4 [31, 32, 47].

### 4.4. Theory study: the MCR-ALS calculations

MCR-ALS aids in resolving the multi-component compounds' mixture toward a simple model. Studies revealed the high capability of MCR-ALS for spectroscopic data analysis of the formation processes of molecular complexes [27, 29]. MCR methods can decompose experimental data matrix (D) into an output of concentration matrix (C) and corresponding spectra (S) through a bilinear model. This model could be shown as an algebraic model (Eq. 7):

$$D = CS^T + E \quad (\text{Eq. 7})$$

The transposition of the matrix is indicated by the superscript T. The residuals matrix (E) must relate to the test error. The MCR-ALS approach is an iterative process in which the S and C are calculated using least squares, and the iterative optimization continues until the model converges. Initial estimates of spectral profiles or concentrations, which can be produced using appropriate methods, are required for the procedure.

Lack of fit (LOF) was employed to evaluate the quality and validity of MCR-ALS. The value of LOF is defined as (Eq. 8):

$$LOF(\%) = 100 \times \sqrt{\frac{\sum_{ij} (d_{ij} - d_{ij}^*)^2}{\sum_{ij} (d_{ij}^*)^2}} \quad (\text{Eq. 8})$$

where  $d_{ij}$  and  $d_{ij}^*$  are the experimental data and the recalculated values using the MCR-ALS technique, respectively. Data matrices were acquired from fluorescence emission, and UV-Vis spectra were integrated into the row and augmented data (column-wise) matrix ( $D_{aug}$ ) according to Eq. 9 [30, 48].

$$D_{aug} = \begin{bmatrix} D_{UV}^{HSA} & D_F^{HSA} \\ D_{UV}^{LET} & D_F^{LET} \end{bmatrix} = \begin{bmatrix} C^{HSA} \\ C^{LET} \end{bmatrix} \begin{bmatrix} S_{UV}^T & S_F^T \end{bmatrix} + \begin{bmatrix} E_{UV}^{HSA} & E_F^{HSA} \\ E_{UV}^{LET} & E_F^{LET} \end{bmatrix} \quad (\text{Eq. 9})$$

The  $D_{UV}$  and  $D_F$  show the spectra data. The MCR-ALS algorithm extracted a matrix of concentration profile (row-wise augmented) and related pure spectra matrix from the  $D_{aug}$  resolution. These simultaneous analyses provide more information than the single analysis defined by Eq. (7).

**Acknowledgements:** The authors would like to thank the Drug applied research center, Tabriz University of medical sciences, Iran, for rendering financial support under grant number 92/82 and 59331 and ethical code of IR.TBZMED.REC.1396.882. Moreover, we thank the Soha company for kindly gifting LET powder.

**Author contributions:** Concept -S.S.; Design - S.S., P.Gh., F.P.; Supervision - S.S.; Resources - S.S.; Materials - S.S.; Data Collection and/or Processing - S.S., P.Gh.; Analysis and/or Interpretation - P.Gh., S.S., F.P.; S.Sh., M.Z.; Literature Search - P.Gh., S.S., F.P.; Writing - P.Gh.; Critical Reviews - S.S.H., S.S., M.Z.

**Conflict of interest statement:** The authors declared no conflict of interest.

## REFERENCES

- [1] Ghuman J, Zunszain PA, Petitpas I, Bhattacharya AA, Otagiri M, Curry S. Structural basis of the drug-binding specificity of human serum albumin. *J Mol Biol.* 2005; 353(1): 38-52. <https://doi.org/10.1016/j.jmb.2005.07.075>
- [2] Yamasaki K, Chuang VTG, Maruyama T, Otagiri M. Albumin-drug interaction and its clinical implication. *Biochim Biophys Acta.* 2013;1830(12):5435-5443. <https://doi.org/10.1016/j.bbagen.2013.05.005>
- [3] Kratz F. Albumin as a drug carrier: Design of prodrugs, drug conjugates and nanoparticles. *J Control Release.* 2008; 132(3): 171-183. <https://doi.org/10.1016/j.jconrel.2008.05.010>
- [4] Baumann K. Cross-validation as the objective function for variable-selection techniques. *Trends Anal Chem.* 2003; 22(6): 395-406. [https://doi.org/10.1016/S0165-9936\(03\)00607-1](https://doi.org/10.1016/S0165-9936(03)00607-1)
- [5] Ajaj KA, Graeser R, Fichtner I, Kratz F. In vitro and in vivo study of an albumin-binding prodrug of doxorubicin that is cleaved by cathepsin B. *Cancer Chemother Pharmacol.* 2009; 64(2): 413-418. <https://doi.org/10.1007/s00280-009-0942-8>
- [6] Kratz F. A clinical update of using albumin as a drug vehicle – A commentary. *J Control Release.* 2014; 190: 331-336. <https://doi.org/10.1016/j.jconrel.2014.03.013>
- [7] Maruyama T, Lin C, Yamasaki K, Miyoshi T, Imai T, Yamasaki M, Otagiri M. Binding of suprofen to human serum albumin: role of the suprofen carboxyl group. *Biochem Pharmacol.* 1993; 45(5): 1017-1026. [https://doi.org/10.1016/0006-2952\(93\)90245-R](https://doi.org/10.1016/0006-2952(93)90245-R)
- [8] Farsad SA, Haghaei H, Shaban M, Zakariazadeh M, Soltani S. Investigations of the molecular mechanism of diltiazem binding to human serum albumin in the presence of metal ions, glucose and urea *J Biomol Struct Dyn.* 2022;40(15):6868-6879. <https://doi.org/10.1080/07391102.2021.1891137>
- [9] Bourassa P, Dubeau S, Maharvi GM, Fauq AH, Thomas TJ, Tajmir-Riahi HA. Binding of antitumor tamoxifen and its metabolites 4-hydroxytamoxifen and endoxifen to human serum albumin. *Biochimie.* 2011; 93(7): 1089-1101. <https://doi.org/10.1016/j.biochi.2011.03.006>
- [10] Kandagal PB, Ashoka S, Seetharamappa J, Shaikh SMT, Jadegoud Y, Ijare OB. Study of the interaction of an anticancer drug with human and bovine serum albumin: Spectroscopic approach. *J Pharm Biomed.* 2006; 41(2): 393-399. <https://doi.org/10.1016/j.jpba.2005.11.037>
- [11] Punith R, Seetharamappa J. Spectral characterization of the binding and conformational changes of serum albumins upon interaction with an anticancer drug, anastrozole. *Spectrochim Acta A Mol Biomol Spectrosc.* 2012; 92:37-41. <https://doi.org/10.1016/j.saa.2012.02.038>
- [12] Sivakumar R, Naveenraj S, Anandan S. Interactions of serum albumins with antitumor agent benzo [a] phenazine—a spectroscopic study. *J Lumin.* 2011; 131(10): 2195-2201. <https://doi.org/10.1016/j.jlumin.2011.05.005>
- [13] Hossain M, Khan AY, Suresh Kumar G. Study on the thermodynamics of the binding of iminium and alkanolamine forms of the anticancer agent sanguinarine to human serum albumin. *J Chem Thermodyn.* 2012; 47: 90-99. <https://doi.org/10.1016/j.jct.2011.09.026>
- [14] Shi Y, Liu H, Xu M, Li Z, Xie G, Huang L, Zeng Z. Spectroscopic studies on the interaction between an anticancer drug ampelopsin and bovine serum albumin. *Spectrochim. Acta A Mol.* 2012; 87: 251-257. <https://doi.org/10.1016/j.saa.2011.11.048>
- [15] Hu W, Luo Q, Wu K, Li X, Wang F, Chen Y. The anticancer drug cisplatin can cross-link the interdomain zinc site on human albumin. *Chem Comm.* 2011; 47(21): 6006-6008. <https://doi.org/10.1039/C1CC11627D>
- [16] Huang S, Zhu F, Qian Q, Xiao Q, Su W. Thermodynamic Investigation of interaction between [(η 6-p-cymene) RuII (Acetone-N 4-phenylthiosemicarbazone) Cl] Cl anticancer drug and human serum albumin: Spectroscopic and electrochemical studies. *Biol Trace Elem Res.* 2015; 164(1): 150-161. <https://doi.org/10.1007/s12011-014-0184-4>
- [17] Ye Z-W, Ying Y, Yang X-l, Zheng Z-q, Shi J-n, Sun Y-f. A spectroscopic study on the interaction between the anticancer drug erlotinib and human serum albumin. *J Incl Phenom Macrocycl Chem.* 2014; 78(1-4): 405-413. <https://doi.org/10.1007/s10847-013-0311-4>
- [18] Haynes BP, Dowsett M, Miller WR, Dixon JM, Bhatnagar AS. The pharmacology of letrozole. *J Steroid Biochem Mol Biol.* 2003; 87(1): 35-45. [https://doi.org/10.1016/S0960-0760\(03\)00384-4](https://doi.org/10.1016/S0960-0760(03)00384-4)
- [19] Lamb HM, Adkins JC. Letrozole. *Drugs.* 1998; 56(6): 1125-1140. <https://doi.org/10.2165/00003495-199856060-00020>
- [20] Miller W, Anderson T, Dixon J. Anti-tumor effects of letrozole. *Cancer Invest.* 2002; 20(S2): 15-21. <https://doi.org/10.1081/CNV-120014882>

- [21] Bhatnagar AS. The discovery and mechanism of action of letrozole. *Breast Cancer Res Treat.* 2007; 105(1): 7-17. <https://doi.org/10.1007/s10549-007-9696-3>
- [22] Annapurna MM, Mohapatro C, Narendra A. Stability-indicating liquid chromatographic method for the determination of letrozole in pharmaceutical formulations. *J Pharm Anal.* 2012; 2(4): 298-305. <https://doi.org/10.1007/s10549-007-9696-3>
- [23] Dombernowsky P, Smith I, Falkson G, Leonard R, Panasci L, Bellmunt J. Letrozole, a new oral aromatase inhibitor for advanced breast cancer: double-blind randomized trial showing a dose effect and improved efficacy and tolerability compared with megestrol acetate. *J Clin Oncol.* 1998; 16(2): 453-461. <https://doi.org/10.1023/A:1008226721932>
- [24] Pfister CU, Martoni A, Zamagni C, Lelli G, De Braud F, Souppart C. Effect of age and single versus multiple dose pharmacokinetics of letrozole (Femara®) in breast cancer patients. *Biopharm Drug Dispos.* 2001; 22(5): 191-197. <https://doi.org/10.1002/bdd.273>
- [25] Maliszewska M, Pozycka J, Szkudlarek A, Chudzik M. Fluorometric investigation on the binding of letrozole and resveratrol with serum albumin. *Protein Pept Lett.* 2016; 23(10): 867-877. <https://doi.org/00000023/00000010/art00004>
- [26] Bijari N, Moradi S, Ghobadi S, Shahlaei M. Elucidating the interaction of letrozole with human serum albumin by combination of spectroscopic and molecular modeling techniques. *Res Pharm Sci.* 2018; 13(4): 304. <https://doi:10.4103/1735-5362.235157>
- [27] Naseri A, Hosseini S, Rasoulzadeh F, Rashidi M-R, Zakery M, Khayamian T. Interaction of norfloxacin with bovine serum albumin studied by different spectrometric methods; displacement studies, molecular modeling and chemometrics approaches. *J Lumin.* 2015; 157: 104-112. <https://doi.org/10.1016/j.jlumin.2014.08.031>
- [28] Zhang G, Zhao N, Wang L. Fluorescence spectrometric studies on the binding of puerarin to human serum albumin using warfarin, ibuprofen and digitoxin as site markers with the aid of chemometrics. *J Lumin.* 2011; 131(12): 2716-2724. <https://doi.org/10.1016/j.jlumin.2011.07.011>
- [29] Mousavi SF, Fatemi MH. Probing the binding mechanism of capecitabine to human serum albumin using spectrometric methods, molecular modeling, and chemometrics approach. *Bioorg Chem.* 2019; 90: 103037. <https://doi.org/10.1016/j.bioorg.2019.103037>
- [30] Manouchehri F, Izadmanesh Y, Aghaee E, Ghasemi JB. Experimental, computational and chemometrics studies of BSA-vitamin B6 interaction by UV-Vis, FT-IR, fluorescence spectroscopy, molecular dynamics simulation and hard-soft modeling methods. *Bioorg Chem.* 2016; 68: 124-136. <https://doi.org/10.1016/j.bioorg.2016.07.014>
- [31] Sadeghinia A, Soltani S, Aghazadeh M, Khalilifard J, Davaran S. Design and fabrication of clinoptilolite-nanohydroxyapatite/chitosan-gelatin composite scaffold and evaluation of its effects on bone tissue engineering. *J Biomed Mater Res A.* 2020; 108(2): 221-233. <https://doi.org/10.1002/jbm.a.36806>
- [32] Haghaei H, Hosseini SRA, Soltani S, Fathi F, Mokhtari F, Karima S. Kinetic and thermodynamic study of beta-Boswellic acid interaction with Tau protein investigated by surface plasmon resonance and molecular modeling methods. *BioImpacts: BI.* 2020; 10(1): 17. <https://doi.org/10.15171/Fbi.2020.03>
- [33] Poureshghi F, Ghandforoushan P, Safarnejad A, Soltani S. Interaction of an antiepileptic drug, lamotrigine with human serum albumin (HSA): Application of spectroscopic techniques and molecular modeling methods. *J Photochem Photobiol Biol.* 2017; 166: 187-192. <https://doi.org/10.1016/j.jphotobiol.2016.09.046>
- [34] Safarnejad A, Shaghghi M, Dehghan G, Soltani S. Binding of carvedilol to serum albumins investigated by multi-spectroscopic and molecular modeling methods. *J Lumin.* 2016; 176: 149-158. <https://doi.org/10.1016/j.jlumin.2016.02.001>
- [35] Zakariazadeh M, Barzegar A, Soltani S, Aryapour H. Developing 2D-QSAR models for naphthyridine derivatives against HIV-1 integrase activity. *Med Chem Res.* 2015; 24(6): 2485-2504. <https://doi.org/10.1007/s00044-014-1305-5>
- [36] Gholizadeh hh S, Karami H, Zakariazadeh M, Shokri J, Soltani S. Mode of binding, kinetic and thermodynamic properties of a lipid like drug (Fingolimod) interaction with human serum albumin. *Bioimpacts.* 2023; 13(2): 109-121. <https://doi.org/10.34172/bi.2022.23383>
- [37] Du W, Teng T, Zhou C-C, Xi L, Wang J-Z. Spectroscopic studies on the interaction of bovine serum albumin with ginkgolic acid: binding characteristics and structural analysis. *J Lumin.* 2012; 132(5): 1207-1214. <https://doi.org/10.1016/j.jlumin.2011.12.067>
- [38] Cui F, Qin L, Zhang G, Liu X, Yao X, Lei B. A concise approach to 1,11-didechloro-6-methyl-4'-O-demethyl rebeccamycin and its binding to human serum albumin: Fluorescence spectroscopy and

- molecular modeling method. *Bioorg Med Chem.* 2008; 16(16): 7615-7621. <https://doi.org/10.1016/j.bmc.2008.07.017>
- [39] Ross PD, Subramanian S. Thermodynamics of protein association reactions: forces contributing to stability. *Biochemistry.* 1981; 20(11): 3096-3102. <https://doi.org/10.1021/bi00514a017>
- [40] Punith R, Katrahalli U, Kalanur SS, Jaldappagari S. Mechanistic and conformational studies on the interaction of anti-inflammatory drugs, isoxicam and tenoxicam with bovine serum albumin. *J Lumin.* 2010; 130(11): 2052-2058. <https://doi.org/10.1111/j.1745-7270.2007.00320.x>
- [41] Kong J, Yu S. Fourier transform infrared spectroscopic analysis of protein secondary structures. *Acta Biochim Biophys Sin.* 2007; 39(8): 549-559. <https://doi.org/10.1111/j.1745-7270.2007.00320.x>
- [42] Venyaminov SY, Kalnin N. Quantitative IR spectrophotometry of peptide compounds in water (H<sub>2</sub>O) solutions. I. Spectral parameters of amino acid residue absorption bands. *Biopolymers.* 1990; 30(13-14): 1243-1257. <https://doi.org/10.1002/bip.360301309>
- [43] Perez-Iratxeta C, Andrade-Navarro MA. K2D2: estimation of protein secondary structure from circular dichroism spectra. *BMC Struct Biol.* 2008; 8(1): 25. <https://doi.org/10.1186/1472-6807-8-25>
- [44] Trott O, Olson AJ. AutoDock Vina: improving the speed and accuracy of docking with a new scoring function, efficient optimization, and multithreading. *J Comput Chem.* 2010; 31(2): 455-461. <https://doi.org/10.1002/jcc.21334>
- [45] Wardell M, Wang Z, Ho JX, Robert J, Ruker F, Ruble J. The atomic structure of human methemalbumin at 1.9 Å. *Biochem Biophys Res Commun.* 2002; 291(4): 813-819. <https://doi.org/10.1006/bbrc.2002.6540>
- [46] Froimowitz M. HyperChem: a software package for computational chemistry and molecular modeling. *Biotechniques.* 1993; 14(6): 1010-1013. <http://pascal-francis.inist.fr/vibad/index.php?action=getRecordDetail&idt=4890712>
- [47] Wallace AC, Laskowski RA, Thornton JM. Thornton, LIGPLOT: a program to generate schematic diagrams of protein-ligand interactions. *Protein Eng.* 1995; 8(2): 127-134. <https://doi.org/10.1093/protein/8.2.127>
- [48] De Luca M, Ragno G, Ioele G, Tauler R. Multivariate curve resolution of incomplete fused multiset data from chromatographic and spectrophotometric analyses for drug photostability studies. *Anal Chim Acta.* 2014; 837: 31-37. <https://doi.org/10.1016/j.aca.2014.05.056>